공학박사 학위논문

Optimal control strategies for gas cooling systems using geometric design and model predictive control

구조 설계와 모델예측제어를 사용하는 기체냉각시스템의 최적 운전전략 수립

2016년 6월

서울대학교 대학원

화학생물공학부

임 유 경

Optimal control strategies for gas cooling systems using geometric design and model predictive control

지도교수 이 종 민

이 논문을 공학박사 학위논문으로 제출함

2016년 12월

서울대학교 대학원

화학생물공학부

임 유 경

임 유 경의 박사 학위논문을 인준함

2016년 6월

위 원 장 이 종 협 (인)

부위원장 이 종 민 (인)

위 원 윤 인 섭 (인)

위 원 이 원 보 (인)

위 원 남 재 욱 (인)

Abstract

Optimal control strategies for gas cooling systems using geometric design and model predictive control

Yu Kyung Lim

School of Chemical and Biological Engineering

The Graduate School

Seoul National University

This thesis presents a theoretical approach on designing the geometry of a gas cooling system unit and its application with the multivariable optimal control technique based on the dynamic mathematical models with a motivation to enhance the cooling efficiency. The gas cooling system can be defined as a process that cools down the exterior heat or solid microparticles introduced to a confined volume space by injecting inert cooling gas stream that absorbs the released heat. Two example cooling processes that are discussed in this study and come under this definition are the CO_2 storage tank pre-cooling process and the microparticle cooling process. Although both processes are included in a same process category, the individual process characteristics and their ultimate goals which need to be achieved are significantly different. Hence, such factors requiring the main consideration are discussed for the design of

the cooling process units. These apply also on developing the optimal controller scheme for the gas cooling systems. Rigorous dynamic modelings are derived for each process based on the first principles which are further used in the development of appropriate model predictive control (MPC) schemes. The result produced by these optimal controllers are later compared with base cases using the proportional-integral (PI) controllers, which illustrate that the multivariable optimal control is able to enhance the stability and the efficiency of both processes.

First example is the pre-cooling process of CO_2 storage tanks. The design of CO_2 storage tanks are determined in advance considering the maximization of the available loading amount. The tank system must be cooled before loading cryogenic liquid CO_2 to prevent physical and thermal damage to the tank wall. The pre-cooling process gasifies a fraction of the liquid CO_2 cargo and injects the resulting gas into the storage tank until the tank reaches the target temperature and pressure. Thus an MPC approach for optimizing the injection flowrate of CO_2 gas to reduce the loss of liquid CO_2 cargo and CO_2 capturing and compression cost is proposed. The process is mathematically formulated into a nonlinear multi-input-multi-output (MIMO) gas-phase system in which the injection mass flowrate and the outlet purging mass flowrate of CO_2 gas act as control inputs. Then, a finite-horizon linearized model predictive control (MPC) scheme is designed to make the tank system reach the target state within a designated operation time limit. A terminal penalty is suboptimally approximated by solving a modified discrete Lyapunov stability condition and added to the control objective function in order

to provide a theoretical finite-horizon stability and enhance the process termination.

For the microparticle cooling process which is the second example, a systematical procedure for selecting a favorite design of a cylinder-on-cone cooling chamber that provides sufficient cooling residence time for spherical polymer particles produced by a prototype polymer melt-spray nozzle is suggested. First, calculations on the particle residence time required for cooling is carried out using a lumped particle model to determine the chamber height. Second, dynamic responses with a step input of the hot air injection rate and the overall air flow streamlines inside the case examples with different chamber structures are obtained with computational fluid dynamics (CFD) simulations. The simulation results suggest that the cone height and the diameters of the cylinder and the outlet interact each other, influencing the mixing and the heat transfer of the gas phase inside the cooling chamber. A chamber design with less instability and good mixing in the air flow is selected among the case designs. CFD simulation results show that polymer droplets are sufficiently cooled in the selected chamber geometry.

Lastly, an adaptive MPC structure controlling the air temperature inside the spray cooling chamber and the flowrate of the purging air out from the chamber outlet simultaneously by manipulating the injection flowrates of cold air and normal air streams is devised. The idea is based on the fact that significant portion of microparticle products depend their moving trajectories on the gravity and the flowrate of the surrounding air stream, which make these two variables the main operation parameters

influencing the efficiencies of the follow-up units which collect the microparticles according to their sizes. We demonstrate that both control variables are well-managed near given setpoints through the MPC application, rejecting three possible scenarios of step disturbances added on the process parameters including the setpoint of the air temperature inside the spray cooling chamber, the surrounding air temperature and the injection mass flowrate of the melt feed stream.

Keywords: Pre-cooling process, Microparticle cooling process, Model predictive control, Computational fluid dynamics

Student Number: 2010-21010

Contents

List of Figures

List of Tables

Chapter 1

Introduction

A gas cooling system is a cooling process that is generally operated inside a confined space volume where heat sources carried by outer materials or exterior energy penetrating through the unit wall are transferred to the surrounding cooling gas stream, which is well-mixed with the heat sources within the cooling unit. Unlike cooling agents such as water or steam, volatile substances including ethanol and fluorine chemicals, the cooling materials used in a gas cooling system regarding this study include nitrogen (N_2), carbon dioxide (CO_2) and air, all of them being chemically inert [4]. Such gases do less damage on properties and shapes of products and reduce the possibility of operation hazards such as fire and explosions, the latter being strictly managed especially in the microparticle producing industries [5]. Despite these advantages, they generally have heat capacities same or lower than the normal air, which can cause following problems at the actual operation and process design stages of gas cooling systems using inert gases. First, cooling efficiency is poor compared to other types of coolants. As an example in a process that cools miscellaneous particles, the size of the process system may

become considerably large in order to provide sufficient length of particle residence time (PRT) inside the cooling unit. Second, the volume of the cooling gas used in process can rise to an extensive amount due to low density, making it difficult to cope with the rising pressure inside process units and increasing the operation cost having to spend more on the cooling power supply. To tackle these problems concerning gas cooling systems, a systematic approach with a theoretical background on designing the geometry of a given gas cooling process unit and application of the optimal control technology which can successfully manipulate multivariable interactions among the process variables are discussed. In this thesis, two process examples including the pre-cooling process of the CO_2 storage tank unit and the microparticle cooling process producing polymer particle products using a melt-spray system are studied following the research topics explained above. Although these processes are loosely connected with each other in the sense that they use similar means of cooling, their ultimate goals are different which require separate point of view in conducting the research. More detailed descriptions and definition of the study objectives are provided in later sections.

Chapter 2

Pre-cooling process of CO_2 storage tank in CCS ship transportation

2.1 Introduction

A CO_2 carrier is a means for transporting liquid CO_2 via ship, which is part of the carbon capture and storage (CCS) chain. Its role is to ship liquid CO_2 waste produced from the onshore CO_2 capture and liquefaction process, transport it to an offshore storage site and support the injection process into suboceanic strata [6]. Although CO_2 carriers are more economical than CO_2 pipelines when the amount of the cargo is small and the shipping distance is greater than approximately 1000 km [7, 8], a case study has shown that the CO_2 transportation cost of CO_2 pipelines is lower than that of CO_2 carriers when the transportation process is limited to the case of South Korea [9]. Therefore, detailed studies on the entire loading/unloading and shipping process operations of CO_2 carriers are necessary to determine their optimal operating conditions and to ensure a competitive edge over the pipeline networks. The pre-cooling process is operated prior to the actual shipping, and this process pushes the tank

pressure and temperature closer to those of liquefied CO_2 cargo with vaporized CO_2, starting from an initial condition of ($300\,$kPa, $293.15\,$K) and shifting towards ($500\,$kPa, $243.15\,$K). The purpose of this process is to protect the stability of the wall material from thermal deformation and to reduce the generation of boil-off gas (BOG) during onloading [10]. In this study, an optimal control problem of the pre-cooling process is formulated to enhance the process efficiency and to reduce the amount of cooling gas injection, since excessive use of cooling gas would lead to the loss of capturing and liquefying cost of CO_2.

In order to find the efficient operation of this process, several important considerations should be taken into account: first, the pressure of the CO_2 storage tank should be controlled in addition to the tank temperature; overpressure of the tank might cause backflow while the liquid CO_2 of a cargo flows into the tank. In contrast, a low tank pressure might result in the excessive generation of boil-off gas during the loading process. Second, the pre-cooling process needs to be completed within a predetermined time because it is advantageous to keep the time spent on waste material transport as short as possible. At the same time, the recommended maximum cooling rate of the storage tank should be kept at approximately $-10\,$K/h to prevent any damage from thermal brittling. Finally, it is necessary to develop a dynamic model of the pre-cooling process and provide an optimal input sequence that controls the tank pressure and temperature while minimizing the injection and outlet purging mass flowrates of the cooling gas.

Previous studies on gas storage tank control systems generally fo-

cus on tank pressure controllers because they are sufficient for regulating the tank temperature due to a self-pressurization effect without requiring additional temperature controllers [11, 12]. For example, BOG regulation for cryogenic liquefied natural gas (LNG) storage tanks has been achieved using single-input-single-output (SISO) proportional-integral-derivative (PID) controllers, which manipulate the outlet purging gas flowrate to maintain the tank pressure, and there has been no need to minimize the outlet purging flowrate because boil-off LNG could be utilized as fuel [13]. From the industrial point of view, the pre-cooling process has been an essential step in the start-up process of on-shore LNG tanks and facilities which comes before the un-loading of the LNG cargo [14, 15]. In a case of the Pyeontaek LNG terminal in South Korea managed by the Korea Gas Corporation (KOGAS), a continuous circulation of low-pressure LNG gas lowers the temperature of the unloading facilities. Since the terminal lines are directly connected to nearby power plants and automobile manufacturing factories, some of the LNG gas used in pre-cooling are utilized as an energy source [16]. By contrast, CO_2 BOG is inherently a waste material, and therefore its outlet purging mass flowrate requires minimization as the CO_2 BOG generation should lower the economic efficiency of the CCS process.

Considering the above, this part of research develops a nonlinear mathematical model of the pre-cooling process of CO_2 storage tanks and calculate an optimal control input sequence using the MPC algorithm to compensate linearization error and handle input constraints. The MPC algorithm has been applied on various industries including Shell

Oil starting from 1970s [17]. Compared to a simple feedback based control, it provides significant improvements in multivariable processes including an LNG plant such as reducing the process output instabilities and increasing profit by pushing the operation condition closer to optimal limit [18]. A terminal penalty must be added to the control objective to form a finite-horizon MPC as well as to complete the process within the time limit. This terminal penalty is obtained by solving a Lyapunov stability condition in the case of a linear state space problem, but this is not possible with a nonlinear problem unless an iterative calculation is adopted [19, 20]. In this study the process system is linearized at the target state for the formation of a linear MPC scheme. However, the system is an integrating process with the target state being a critical equilibrium. Since the terminal penalty is difficult to obtain through the Lyapunov stability condition in such a case, this study uses a suboptimal method to approximate the weighting matrix of a quadratic terminal penalty. Several candidates of the weighting matrix of the terminal penalty are obtained by solving a modified linear Lyapunov stability condition in which a slack variable is added. We select four of these candidates that satisfies the original nonlinear Lyapunov stability condition. Some results from this suboptimal selection occasionally destabilize the MPC because the resulting terminal penalty terms are large compared to other terms in the control objective; hence, the effects of the value of the terminal penalty on the resulting optimal input and output sequences are also considered. Finally the MPC results are compared with a base case of the proportional-integral (PI) control application in order to demonstrate that

the MPC is more advantageous in securing the process stability than the PI controller.

2.2 Process description

Design of the storage tank geometry must consider the fact that the tank system shall eventually be installed on board. Therefore its blueprints confirmed by the contractors in advance focus mainly on maximizing the loading amount of liquid CO_2 cargo within a confined space volume, rather than considering the pre-cooling process which is one of the intermediary step during the tank pretreating procedure. Taking such factors into account, the tank is designed in a bi-lobe shape with maximum capacity of $13\,000\,\mathrm{m}^3$. A pilot experiment including two down-scaled bi-lobe tanks with a capacity of $40\,\mathrm{m}^3$ each depicted in Fig. 1 was conducted in 2013 in order to analyze the BOG generation when the tanks operate in a cryogenic condition while the exterior surrounding had room temperature [1].

A desirable operating scenario regarding the pre-cooling process is to inject CO_2 cooling gas at $225.15\,\mathrm{K}$ into a tank initially filled with CO_2 to increase the tank pressure from $300\,\mathrm{kPa}$ to $500\,\mathrm{kPa}$ and to cool the storage tank temperature from $293.15\,\mathrm{K}$ to $243.15\,\mathrm{K}$, where the main operating unit in the pre-cooling process is the CO_2 storage tank with an ellipsoidal shape in the horizontal direction. Fig. 2 shows a simplified process flow diagram that includes the storage tank and the peripheral units. The tank wall is composed of carbon steel, and its outer surface is

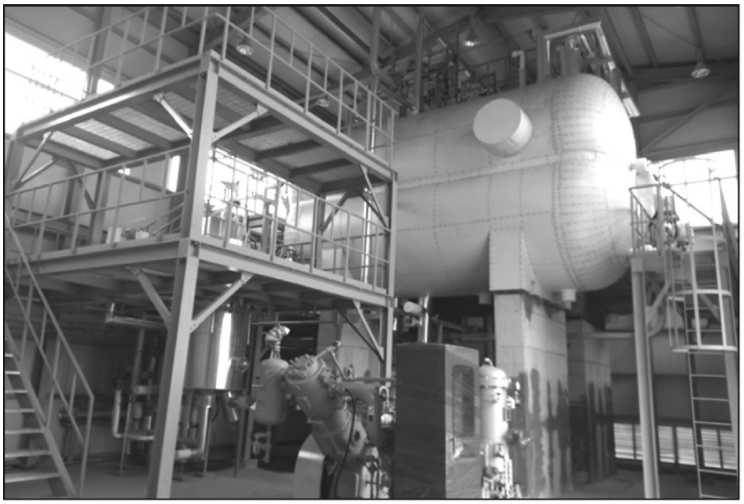

Figure 1: In-door pilot experiment of CO_2 storage tank operation measuring BOG generation [1]

covered with polyurethane spray foam, which acts as the insulation layer of the cryogenic tank.

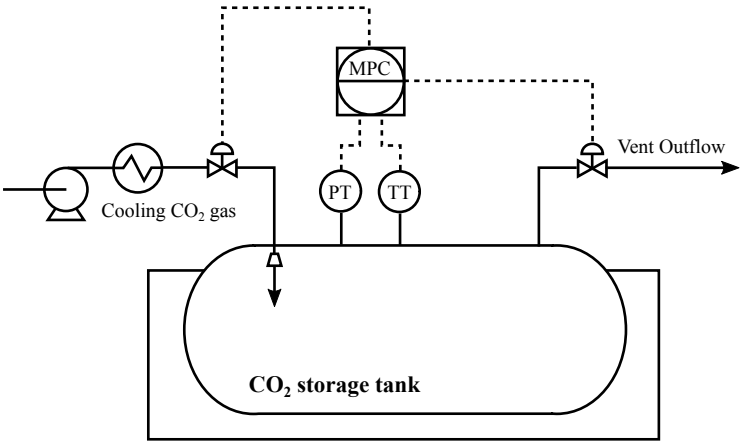

Figure 2: Schematic diagram of the CO_2 storage tank and the pre-cooling process

The actual pre-cooling process involves a tank system in which the tank pressure and temperature are defined non-ideally. An analysis of the

system with a high accuracy could be provided by a commercial process simulator by iteratively solving a cubic equation of state such as the Peng-Robinson equation. However, an equally important objective of this study besides the accuracy is to provide a clear analysis on how the state variables interact thermodynamically with the heat sources added to the system. Since such information is difficult to obtain from simulator models, a mathematical model comprised of ordinary differential equations (ODEs) describing the dynamics of the state variables is newly developed based on the mass and energy balances. As our method of developing the mathematical model involves a step that differentiates the equation of state, the ideal gas law is employed in order to simplify the differentiation step and the resulting ODEs. The usage of the ideal gas law is verified by comparing the value of the compressibility factors Z of both the Peng-Robinson equation and the ideal gas law and using a simulation result from a process simulator environment in the later sections.

An additional consideration is given to the specific heat capacity of CO_2. The functional relationship between the specific heat, the temperature and the pressure is identified based on a published experimental data. Other minor assumptions are given at the end of this section.

2.3 Process dynamic model

A mathematical model of the pre-cooling process is required in order to develop an optimal control scheme. The first part of this section shows the steps for developing nonlinear differential equations that describe the

system dynamics based on the mass and energy balances and the ideal gas law. The reliability of this mathematical model is tested in the second part by comparing the open-loop step responses with those of a commercial process simulator.

2.3.1 Mathematical model

The Peng-Robinson equation of state is common choice for the thermodynamic modeling of cryogenic liquid-gas systems, such as LNG storage tanks [21, 22]. This equation of state produces more accurate thermodynamic values for this particular circumstance than the ideal gas law. The Peng-Robinson equation of state and the ideal gas law are stated in Eqs. (2.1a-2.1b), respectively, where P is the pressure, T is the temperature, R is the ideal gas constant, and V_m is the molar volume. Detailed descriptions of other accompanying parameters in Eq. (2.1a) are provided in [23].

$$P = \frac{RT}{V_m - b} - \frac{a\,(T)}{V_m\,(V_m + b) + b\,(V_m - b)} \tag{2.1a}$$

$$P = \frac{RT}{V_m} \tag{2.1b}$$

When the condition of a CO_2 storage tank changes from the initial state ($300\,\text{kPa}$, $293.15\,\text{K}$) to the target state ($500\,\text{kPa}$, $243.15\,\text{K}$), the compressibility factor $Z = \frac{PV_m}{RT}$ calculated using the Peng-Robinson equation of state changes from 0.9826 to 0.9487. These values are close to one and therefore employing Eq. (2.1b) for the thermodynamic modeling is re-

garded as valid. Justification of the use of the ideal gas law in a cryogenic gas system by calculating the value of Z is also stated in [24]. We compromise the model accuracy and consider that the ideal gas law is sufficient for describing the general tendency of the change in the tank dynamics.

As for the specific heat capacity inside a system with a constant volume, it is originally derived from the specific internal energy that is expressed as a function of temperature and volume [25]. The differentiated specific internal energy is shown in Eq. (2.2),

$$dU = \left(\frac{\partial U}{\partial T}\right)_V dT + \left(\frac{\partial U}{\partial V}\right)_T dV \tag{2.2}$$

where $C_v = \left(\frac{\partial U}{\partial T}\right)_V$ is the specific heat capacity at a constant V. The value of C_v should theoretically depend only on T when the gas is supposed to be ideal. However this is not directly usable in our case with a non-ideal cooling gas. Hence the specific heat capacity inside the tank system is defined as a function of T and P. For this study, experimental measurements of C_p of CO_2 within the range between 0.5 bar - 20 bar and 200 K - 700 K from [26] are used to fit a 5^{th}-order polynomial function of T and P, as shown in Eq. (2.3). Later the values of C_p are multiplied by a constant value to result in the corresponding values of C_v. The coefficients calculated by least squares are shown in Table 1. The sum of squared errors (SSE) and R-squared values of Eq. (2.3) are 0.1138 and 0.9708, respectively, whereas a higher-order fitting with either P or T does not lead to a meaningful improvement. The resulting function

shown in Fig. 3 indicates that Eq. (2.3) shows an acceptable agreement with the literature data.

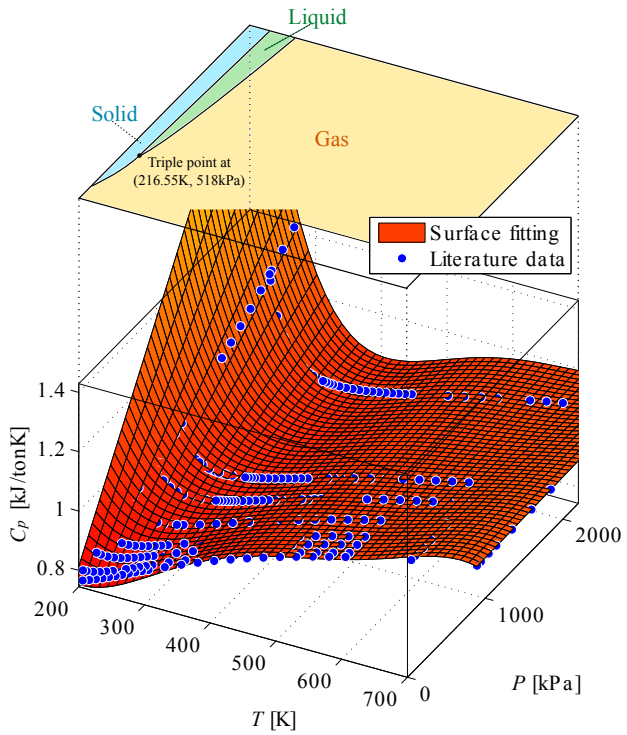

Figure 3: Surface fitting of the heat capacity of CO_2 as a function of temperature and pressure depicted with the CO_2 P-T phase diagram

$$
\begin{aligned}
C_p =& g\left(T, P\right) \\
=& a_{0,0} + a_{0,1}T + a_{0,2}T^2 + a_{0,3}T^3 + a_{0,4}T^4 + a_{0,5}T^5 \\
&+ a_{1,0}P + a_{1,1}PT + a_{1,2}PT^2 + a_{1,3}PT^3 + a_{1,4}PT^4
\end{aligned}
\tag{2.3}
$$

Further assumptions used for modeling are as follows:

Table 1: The polynomial fitting coefficients for C_p in Eq. (2.3)

Coefficient	Value	Coefficient	Value
$a_{0,0}$	1.968×10^{3}	$a_{1,0}$	3.129
$a_{0,1}$	-18.14	$a_{1,1}$	-2.303×10^{-2}
$a_{0,2}$	9.282×10^{-2}	$a_{1,2}$	6.255×10^{-5}
$a_{0,3}$	-2.078×10^{-4}	$a_{1,3}$	-7.388×10^{-8}
$a_{0,4}$	2.175×10^{-7}	$a_{1,4}$	3.197×10^{-11}
$a_{0,5}$	-8.665×10^{-11}		

- The amount of cooling gas condensed to liquid is negligible. In addition the tank system is initially in a single-element (CO_2) gas phase because it is assumed that the tank undergoes a moisture drying process by injecting the CO_2 gas to replace the air with moisture.

- The storage tank does not make direct contact with cradle supports. Therefore, the heat flowrate into the tank through the walls is assumed to be equal at every location of the tank walls.

- The difference between the temperature of the inner and outer sides of the steel layer of the tank wall is negligible because the heat transfer resistance of the steel layer is significantly less than that of the insulation layer.

The mathematical model includes ODEs of the tank pressure P and temperature T, which are derived from the mass and energy balances of the tank system shown in Eqs. (2.4a-2.4d), where M and E are the total amount of mass and energy inside the tank, respectively; q is the external heat source term; m_{in} is the rate of the injection mass flowrate; m_{out} is the rate of outlet purging mass flowrate; e_{in} and e_{out} are the specific

enthalpies of injection and outlet purging streams of the storage tank, respectively; $C_{p,in}$ and T_{in} are the specific heat capacity and the temperature of the injection stream, respectively; C_p and T are the specific heat capacity and the temperature of the tank inside and the outlet purging stream, respectively; P_{ref} is the reference pressure and T_{ref} is the reference temperature.

$$\frac{dM}{dt} = m_{in} - m_{out} \tag{2.4a}$$

$$\frac{dE}{dt} = e_{in} - e_{out} + q \tag{2.4b}$$

$$e_{in} - e_{out} = m_{in} \int_{P_{ref}}^{P_{in}} \int_{T_{ref}}^{T_{in}} C_p dT dP - m_{out} \int_{P_{ref}}^{P} \int_{T_{ref}}^{T} C_p dT dP \tag{2.4c}$$

Equations for q are shown in Eqs. (2.5a-2.5b). u is the overall heat transfer coefficient, which is a function of T_{ex}, the temperature of the external environment; h_{ex} is the external heat convection coefficient; L_{ins} is the thickness of the insulation layer of the tank wall; k_{ins} is the heat conductivity of the insulation layer; h_{tank} is the convective heat transfer coefficient inside the tank; L_{stl} is the thickness of the steel layer of the tank wall; and k_{stl} is the heat conductivity of the steel layer. T_{w1} in Eq. (2.5c) is the temperature of the steel layer. It is derived by rearranging Eq. (2.5a) and can be separately calculated after the value of T is obtained at each

time step.

$$\frac{q}{A} = u\left(T_{ex} - T\right) = h_{tank}\left(T_{w1} - T\right) \tag{2.5a}$$

$$u = \frac{1}{1/h_{ex} + L_{ins}/k_{ins} + L_{stl}/k_{stl} + 1/h_{tank}} \tag{2.5b}$$

$$T_{w1} = T + \frac{u}{h_{tank}}\left(T_{ex} - T\right) \tag{2.5c}$$

Above definitions of mass and energy balances can be related to the ODEs of P and T by converting the ideal gas law in Eq. (2.6) as functions of M and T, where M_g is the molar mass and V is the tank volume.

$$PV = \frac{M}{M_g}RT \tag{2.6}$$

Eq. (2.6) is modified and differentiated in time considering V being constant, resulting Eq. (2.7a) and Eq. (2.7b).

$$\frac{dM}{dt} = \frac{VM_g}{R}\frac{d}{dt}\left(\frac{P}{T}\right) \tag{2.7a}$$

$$\frac{d\left(MT\right)}{dt} = \frac{VM_g}{R}\frac{dP}{dt} \tag{2.7b}$$

The mass balance in Eq. (2.4a) is then combined with Eq. (2.7a) to produce the dynamic model equation of T in Eq. (2.8).

$$\frac{dT}{dt} = \frac{T}{P}\frac{dP}{dt} - \frac{R}{VM_g}\frac{T^2}{P}\left(m_{in} - m_{out}\right) \tag{2.8}$$

Eq. (2.9) is the first step for deriving $\frac{dP}{dt}$. It shows that $\frac{dE}{dt}$ in Eq. (2.4b) is

alternatively defined as the dynamic accumulation of energy in the tank system and arranged to derive $\frac{d(MT)}{dt}$ and $\frac{dC_v}{dt}$, where C_v is the the specific heat capacity in a constant volume. Then, $\frac{d(MT)}{dt}$ and $\frac{dE}{dt}$ in Eq. (2.9) are replaced with the right-hand sides of Eq. (2.7b) and Eq. (2.4b), leading to Eq. (2.10).

$$\frac{dE}{dt} = \frac{d\left(MC_vT\right)}{dt} = C_v\frac{d\left(MT\right)}{dt} + MT\frac{dC_v}{dt} \tag{2.9}$$

$$C_v\frac{d\left(MT\right)}{dt} = \frac{VM_g}{R}\left(C_v\frac{dP}{dt}\right) = -\frac{VM_g}{R}\left(P\frac{dC_v}{dt}\right) + e_{in} - e_{out} + q \tag{2.10}$$

C_v is replaced by C_p with a new constant γ, which is defined as follows:

$$\gamma = \frac{C_p}{C_v} \tag{2.11}$$

where γ is 1.3 for the ideal CO_2 gas. Then, Eq. (2.10) is rearranged into Eq. (2.12), describing $\frac{dP}{dt}$. For $\frac{dC_p}{dt}$, we use Eq. (2.13), which is Eq. (2.3) differentiated in time.

$$\frac{dP}{dt} = -\frac{P}{C_p}\frac{dC_p}{dt} + \frac{1.3R}{VM_gC_p}\left\{e_{in} - e_{out} + uA\left(T_{ex} - T\right)\right\} \tag{2.12}$$

$$\frac{dC_p}{dt} = \frac{d\left\{g\left(T,P\right)\right\}}{dt} \tag{2.13}$$

Finally, Eqs. (2.8), (2.12) and (2.13) are combined to form a system of implicit ODEs representing the dynamics of the pre-cooling process in-

side a tank with a constant volume.

$$\frac{d}{dt}\begin{bmatrix} P \\ T \end{bmatrix} = \begin{bmatrix} -\frac{P}{C_p}\frac{dC_p}{dt} + \frac{1.3R}{VM_gC_p}\left\{e_{in} - e_{out} + uA\left(T_{ex} - T\right)\right\} \\ \frac{T}{P}\frac{dP}{dt} - \frac{R}{VM_g}\frac{T^2}{P}\left(m_{in} - m_{out}\right) \end{bmatrix} \tag{2.14}$$

If the tank system is well insulated, the main driving forces that change P and T are the enthalpy values relevant to m_{in} and m_{out}. The right-hand side of $\frac{dP}{dt}$ shows that P rises when T is lowered as the result of increasing m_{in}. However, the negative second term on the right-hand side of $\frac{dT}{dt}$ shows that its absolute value is reduced by increasing P in the denominator. Injecting cooling gas excessively and increasing P have advantages since they prevent BOG formation during the actual loading afterwards. However the mathematical model indicates that letting P to be increased indefinitely does not have a positive effect on the efficiency of the pre-cooling process, rather wasting the cooling gas. As a result the model shows the interaction between P and T of the storage tank and describes how these variables may be controlled by the potential manipulated inputs m_{in} and m_{out}, whereas such an explanation of the process is difficult to obtain with black box models in commercial process simulators.

2.3.2 Dynamic model verification

The reliability of the model should be verified with experimental data. However because thermodynamic experimental data of the CO_2 storage tank during the pre-cooling process is not available, the accuracy of the mathematical model is validated by comparing two example cases

of the open-loop simulation results from Eq. (2.14) and the process flow diagram (PFD) in Aspen HYSYS 7.3 environment in Fig. 4. The main purpose of the test is to verify whether it is acceptable to use the assumption of the ideal gas law in developing Eq. (2.14). For the Aspen HYSYS 7.3 simulations, the Peng-Robinson equation of state is employed. The valve opening of V2 in Fig. 4 is set to zero since the condensed liquid CO_2 is not released from the storage tank in a real pre-cooling process.

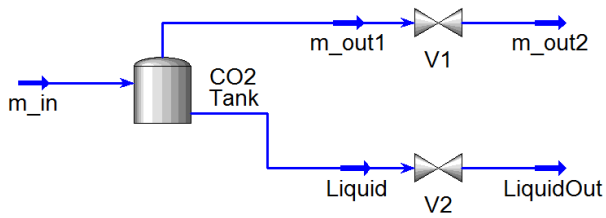

Figure 4: PFD of the pre-cooling process on Aspen HYSYS 7.3

The initial condition of Case 1 is 101.3 kPa, 293.15 K, and the initial condition of Case 2 is 300.0 kPa, 278.15 K. m_{in} and m_{out} in both cases are initially zero, which are changed to 12 ton/h and 10 ton/h respectively when the dynamic simulation starts. The other operating parameters are specified in Table 2. Fig. 5 presents the result of open-loop step response. We conclude that the mathematical model exhibits an acceptable agreement with the results of Aspen HYSYS 7.3 and a satisfactory description of the process dynamics despite using the ideal gas law.

Table 2: Operating parameters of the open-loop step response test

Parameter	Description	Value
A	Outer surface area of tank [m^2]	2.026×10^3
$C_{p,in}$	Specific heat capacity of CO_2 [kJ/ton/K]	824.61
L	Thickness of tank wall insulation layer (polyurethane) [m]	0.30
M_g	Molar weight of CO_2 [ton/kmole]	44.01×10^{-3}
R	Ideal gas constant [kJ/kmole/K]	8.3145
T_{ex}	External environment temperature [K]	293.15
T_{in}	Mass inflow temperature [K]	225.15
V	Tank volume [m^3]	1.30×10^4
h_{ex}	External heat convection coefficient [kJ/m^2/h/K]	10.44
h_{tank}	Internal heat convection coefficient [kJ/m^2/h/K]	15.00
k	Heat conductivity of tank wall insulation layer [kJ/m/h/K]	7.92×10^{-2}

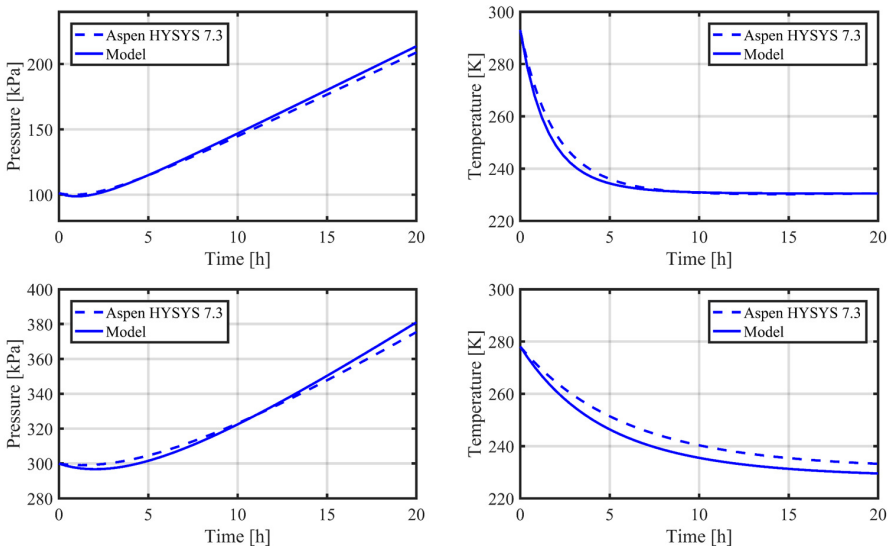

Figure 5: Open-loop step response test with the proposed model and Aspen HYSYS 7.3 ($m_{in} = 12$ ton/h, $m_{out} = 10$ ton/h); (a) tank pressure in Case 1; (b) tank temperature in Case 1; (c) tank pressure in Case 2; (d) tank temperature in Case 2

2.4 Control problem formulation

This section presents two parts to obtain an open-loop optimal input sequence using MPC that adjusts the tank pressure and temperature

from the initial state to the target state. The first part shows a linearized discrete-time model system and the formulation of a control problem. In order to obtain a quadratic terminal penalty term which is required to attract the state variables towards the target state within the fixed operational time, the second part of this section describes a method for approximating a non-unique weighting matrix Q_t of the terminal penalty using a modified Lyapunov stability condition. The modified Lyapunov stability condition can produce a set of suboptimal Q_t candidates when the target state equilibrium is not asymptotically stable.

2.4.1 Discrete MPC

The controller is formulated based on the linearization of the original nonlinear system in Eq. (2.14). Let $\mathbf{x}$ and $\mathbf{u}$ define the state and input vectors, where $\mathbf{x} \in \Re^2$ and $\mathbf{u} \in \Re^2$.

$$\mathbf{x} = \begin{bmatrix} P \\ T \end{bmatrix} = \begin{bmatrix} x_1 \\ x_2 \end{bmatrix}, \quad \mathbf{u} = \begin{bmatrix} m_{in} \\ m_{out} \end{bmatrix} = \begin{bmatrix} u_1 \\ u_2 \end{bmatrix} \tag{2.15}$$

Hence, Eq. (2.14) is represented as a state space model with an initial state $\mathbf{x}_0$ where $\mathbf{u}$ is subject to an input constraint set U for a feasible operation.

$$\begin{aligned} \frac{d\mathbf{x}}{dt} &= \mathbf{f}\left(\mathbf{x}, \mathbf{u}\right) = \begin{bmatrix} f_1 \\ f_2 \end{bmatrix} \\ \mathbf{x}\left(0\right) &= \mathbf{x}_0, \quad \mathbf{u} \in U, \quad \forall t \geq 0 \end{aligned} \tag{2.16}$$

Eq. (2.16) undergoes Jacobian linearization at the target state $\mathbf{x}_t$, where $A := \frac{\partial \mathbf{f}}{\partial \mathbf{x}}\big|_{(\mathbf{x}_t, \mathbf{u}_t)}$ and $B := \frac{\partial \mathbf{f}}{\partial \mathbf{u}}\big|_{(\mathbf{x}_t, \mathbf{u}_t)}$. The system is expected to reach a steady state equilibrium at the target state. The system is further discretized with a sample time of Δt under the zero-order-hold assumption of $\mathbf{u}$, resulting in Eq. (2.17).

$$\mathbf{x}_{k+1} = \Phi \mathbf{x}_k + \Gamma \mathbf{u}_k, \quad (k = 0, 1, 2, \cdots) \tag{2.17}$$

The finite-horizon objective function is defined in Eq. (2.18) [27, 28, 29, 30], where the diagonal matrices $Q \in \Re^{2\times 2}$, $R \in \Re^{2\times 2}$ and $Q_t \in \Re^{2\times 2}$ are the weight matrices for the quadratic penalty terms of $\mathbf{x}_k$ and $\mathbf{u}_k$ and for the terminal penalty, respectively. We assume that the prediction and control horizons have the same length p and that $\mathbf{u}_k$ has zero value for $k \geq p$.

$$\begin{aligned}
J(\mathbf{x}_p, \mathbf{u}_p) &= \min_{\mathbf{x}(\cdot), \mathbf{u}(\cdot)} \sum_{k=0}^{p-1} \left(\mathbf{x}_k^T Q \mathbf{x}_k + \mathbf{u}_k^T R \mathbf{u}_k \right) + \mathbf{x}_p^T Q_t \mathbf{x}_p \\
s.t. \quad \mathbf{u}_k &\in U, \quad p > k \geq 0 \\
\mathbf{u}_k &= \mathbf{0}, \quad k \geq p \\
\mathbf{x}_{k+1} &= \Phi \mathbf{x}_k + \Gamma \mathbf{u}_k, \quad \forall k \\
\mathbf{x}(0) &= \mathbf{x}_0
\end{aligned} \tag{2.18}$$

2.4.2 Modified Lyapunov stability condition

The terminal penalty $V(\mathbf{x}_p) = \mathbf{x}_p^T Q_t \mathbf{x}_p$ provides an upper bound of an infinite horizon cost of the objective function.

$$\sum_{k=p}^{\infty} \left(\mathbf{x}_k^T Q \mathbf{x}_k\right) \leq \mathbf{x}_p^T Q_t \mathbf{x}_p \tag{2.19}$$

Then $V(\mathbf{x}_p)$ is a Lyapunov function that satisfies the Lyapunov stability condition in Eq. (2.20) around the target state $\mathbf{x}_t$. Note that. Eq. (2.20) is the rearrangement of Eq. (2.19). The Lyapunov function $V(\mathbf{x}_p)$ must be positive semi-definite and decrease with time index k, satisfying Eq. (2.20) in a neighborhood Ω, where $\mathbf{x}_t \in \Omega \subset \Re^2$. In order to obtain a solution of Eq. (2.20) at the target state $\mathbf{x}_t$, $\mathbf{x}_t$ is substituted for $\mathbf{x}_p$ later on [31, 32].

$$\begin{aligned} \mathbf{x}_{p+1}^T Q_t \mathbf{x}_{p+1} - \mathbf{x}_p^T Q_t \mathbf{x}_p &\leq -\mathbf{x}_p^T Q \mathbf{x}_p \\ 0 &\leq \mathbf{x}_p^T Q_t \mathbf{x}_p \end{aligned} \tag{2.20}$$

If the eigenvalues of Φ stay inside the unit circle with $|\mathbf{Re}\{\lambda_{\max}(\Phi)\}| < 1$, the target state $\mathbf{x}_t$ where the linearization is executed is an asymptotically stable equilibrium point enabling Eq. (2.20) to be solved directly, producing a unique positive definite Q_t with a positive definite Q. However, if the target state is not asymptotically stable, Eq. (2.20) will not yield a feasible solution. For example, when $|\mathbf{Re}\{\lambda_{\max}(\Phi)\}| = 1$ for some eigenvalues of Φ, the equilibrium induced by such a system is defined as the critical equilibrium. Such system lacking the asymptotical

stability is known as an integrating process. In other words, it is a non self-regulating process. And this trait is common in the process systems industry including supply chains, tanks with an outlet and batch distillation columns [33]. Since the tank pre-cooling process is also an integrating process, it is not possible to utilize the Lyapunov stability condition at its original form. Hence, based on an approach proposed by [34] that developed a continuous MPC algorithm providing a terminal penalty with a guaranteed stabilized terminal region around the target state for a nonlinear system with a nonlinear system which becomes stable when linearized, Eq. (2.20) is altered as follows.

Eq. (2.20) is modified so that it yields a set of suboptimal Q_t matrices at the critical equilibrium. First, $\mathbf{x}_{p+1}$ in Eq. (2.20) is substituted with $(\Phi + \kappa\mathbf{I})\,\mathbf{x}_p$, where κ is an auxiliary slack variable and $\mathbf{I} \in \Re^{2\times 2}$ is the identity matrix. Then, $\mathbf{x}_p$ is eliminated from both sides of Eq. (2.20) to produce Eq. (2.21).

$$\begin{aligned} (\Phi + \kappa\mathbf{I})^T \bar{Q}_t (\Phi + \kappa\mathbf{I}) - \bar{Q}_t &\leq -Q \\ |\lambda(\Phi) + \kappa| &< 1 \end{aligned} \tag{2.21}$$

Then $\bar{Q}_t$, the solution of Eq. (2.21), is a positive definite matrix given that the eigenvalues of $\Phi + \kappa\mathbf{I}$ are inside the unit circle [35]. The range of κ in Eq. (2.21) can be specified using the minimum and maximum values of $\lambda(\Phi)$ and further arranged as the inequality constraint in Eq. (2.22). Since all $\lambda(\Phi)$ must satisfy $|\lambda(\Phi) + \kappa| < 1$ in Eq. (2.21), κ should be located in the intersection of the first two sets shown in Eq. (2.22). We can

obtain several different values of $\bar{Q}_t$ by changing κ within the constraint. Then $\bar{Q}_t$ substitutes for Q_t in the original Lyapunov stability condition in Eq. (2.20). Ω is defined as the region around the equilibrium where Eq. (2.20) is feasible with the suboptimal $\bar{Q}_t$.

$$\begin{aligned} \alpha &= \{\kappa | -1 - \lambda_{\min}(\Phi) < \kappa < 1 - \lambda_{\min}(\Phi)\} \\ \beta &= \{\kappa | -1 - \lambda_{\max}(\Phi) < \kappa < 1 - \lambda_{\max}(\Phi)\} \\ \alpha \cap \beta &= \{\kappa | -1 - \lambda_{\min}(\Phi) < \kappa < 1 - \lambda_{\max}(\Phi)\} \end{aligned} \tag{2.22}$$

This modification is allowed when the system is assumed to be autonomous after a sufficiently long prediction horizon. Otherwise, the feedback input $\mathbf{u}_p = l(\mathbf{x}_p)$ must be included in Eq. (2.21), having a potentially destabilizing effect on solving the control problem with a system that is not asymptotically stable. The feasibility of the neighborhood Ω could be restricted because the choice of $\bar{Q}_t$ is based on the $(\Phi + \kappa\mathbf{I})\mathbf{x}_p$ which is different from $\Phi\mathbf{x}_p$.

Two considerations need to be taken into account before selecting a particular $\bar{Q}_t$. First, state trajectories should stay inside Ω that results from the corresponding $\bar{Q}_t$. Second, $\bar{Q}_t$ having a large value will result in a large $V(\mathbf{x}_p)$ and Ω, but it will consequently destabilize the controller [34]. Therefore the feasibility of Ω and the effect of $V(\mathbf{x}_p)$ on the state trajectories should be checked for each different $\bar{Q}_t$.

2.4.3 PI control

Efficiency of the MPC algorithm on the pre-cooling process is tested against a base case of the proportional-integral (PI) control scheme. As a feedback control method, a PI controller produces subsequent control actions straightforwardly based on the present error between the process output and the setpoint value. It is a linear combination of the proportional and the integral controllers. The control action calculated by the proportional controller is proportionally dependent on the present error which leads to a steady-state offset between the output and the setpoint due to the fact the proportional controller is inherently inactive when the present error term reaches zero. To overcome this condition, the integral controller can accompany the proportional controller in order to add the accumulating error terms generated during the entire operation period to the calculation and compensate for the otherwise insufficient control action. The PI control form for a discrete process system is given by Eq. (2.23), where u_k is the control action at $t = k$; $\bar{u}$ is the nominal control action at the initial steady state; K_c is the proportional controller gain; K_I is the integral controller gain; e_k is the deviation between the process output and the setpoint at $t = k$; Δt is the sampling period, and τ_I is the integral time which is an adjustable parameter depending on the

process time delay [36].

$$
\begin{aligned}
u_k &= \bar{u} + K_c \left(e_k + \frac{\Delta t}{\tau_I} \sum_{j=1}^{k} e_j \right) \\
K_I &= \frac{K_c}{\tau_I}
\end{aligned}
\tag{2.23}
$$

The closed-loop stability for an integrating process is generally more difficult to achieve than for other self-regulating systems. Thus in a control scheme involving an integrating process, the Internal Model Control (IMC) tuning method is able to provide an acceptable control quality in the sense that the user may adjust the aggressiveness and the robustness of the control response with an user-defined time constant [33, 37]. In this study, the controller parameters including K_c and τ_I are adjusted by the IMC tuning method for integrating processes proposed by [2]. The relevant tuning rule for the PI controller is shown in Eq. (2.24a-2.24c), where K_p is the process gain; τ_p is the process time delay and τ_c is the user-defined closed-loop time constant. Note that the numerical constant in Eq. (2.24c) used in the derivation of τ_c is modified to 2000 from 10 proposed by [3] in order to enhance the robustness of the control performance.

$$
\begin{aligned}
K_c &= \frac{1}{K_p} \frac{2\tau_c + \tau_p}{(\tau_p + \tau_c)^2} && \text{(2.24a)} \\
\tau_I &= 2\tau_c + \tau_p && \text{(2.24b)} \\
\tau_c &= \tau_p \sqrt{2000} && \text{(2.24c)}
\end{aligned}
$$

We use a dynamic relative gain array (DRGA) result for configuring the control loop pairings having a relative gain array (RGA) value close to 1, which indicates that the intended control loop has strong controllability, whereas the other configuration does not. DRGA measures the dynamic interactions within multivariable processes [38], occasionally deriving more efficient control structures than the steady-state RGA results. [39] showed in a distillation control problem, that a control configuration with an infinite steady-state value of the RGA provided a good control efficiency, which was predicted by the high-frequency RGA value close to 1.

First, step inputs and responses on both process outputs shown in Fig. (6) are fitted into a transfer function in Eq. (2.25) by using 'tfest' function in MATLAB 2015a.

$$\begin{bmatrix} P \\ T \end{bmatrix} = \begin{bmatrix} \frac{-2236s+0.4331}{s^2+1.605s+0.004292} & \frac{9123s+6.868}{s^2+3.289s+0.005147} \\ \frac{1.049\times10^4 s-0.5323}{s^2+7.635s+0.0008983} & \frac{-727.9s+1.042}{s^2+4.212s+0.0005245} \end{bmatrix} \begin{bmatrix} m_{in} \\ m_{out} \end{bmatrix} \tag{2.25}$$

Eq. (2.25) is then plotted against a logscale frequency interval to result in the DRGA analysis in Fig. (6). The DRGA analysis illustrates that the acceptable control loop pairings are off-diagonal, which are (P, m_{out}) and (T, m_{in}).

Finally, K_p of the integrating process is determined as the average value of the response gains by following Eq. (2.26), where Δu^* is Δu divided by the length of the allowed range of u and Δy^* is Δy divided by the length of the allowed range of y. The resulting control parameters

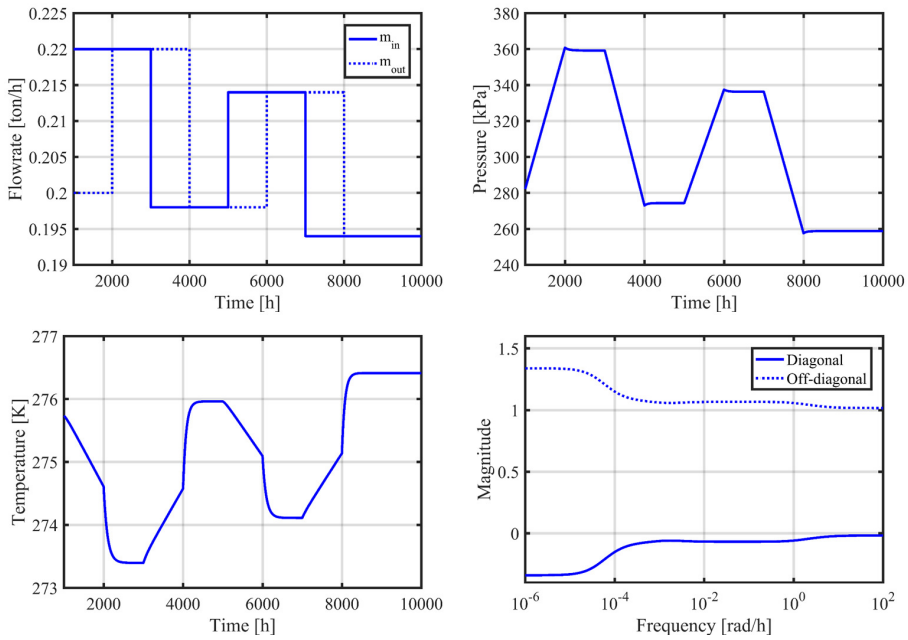

Figure 6: Step responses and dynamic RGA results of the pre-cooling process; top left: step input trajectories of m_{in} and m_{out}, top right: step response trajectory of P; bottom left: step response trajectory of T; bottom right: dynamic RGA based on Eq. (2.25)

are shown in Table 3 where $u_{\max} - u_{\max}$ is 0.2 ton/hr for both m_{in} and m_{out}; $y_{\max} - y_{\max}$ for P and T are 900 kPa and 75 K, respectively and Δt is 0.5h.

$$\begin{aligned} \Delta u^* &= \frac{\Delta u}{u_{\max} - u_{\min}} \\ \Delta y^* &= \frac{\Delta y}{y_{\max} - y_{\min}} \\ K_p &= \frac{\Delta y^*}{\Delta t \Delta u^*} \end{aligned} \tag{2.26}$$

Table 3: Control parameters based on [2, 3]

Control loop	K_p	τ_p	K_c	τ_I	K_I
(P, m_{out})	-9.042e-4	130	-0.3681	1.176e4	-3.130e-5
(T, m_{in})	-1.633e-4	220	-1.204	1.990e4	-6.051e-5

2.5 Dynamic simulation results

In this section, the control performances of the discrete MPC and the PI controller which are illustrated in Sec. 2.4.1 and Sec. 2.4.3, respectively are compared with the proposed pre-cooling process of the CO_2 storage tank. As a result, the MPC control input sequences are influenced by the magnitude of the terminal penalty. Both control algorithms are able to terminate the process within the designated operation time limit, however unlike the MPC result, the trajectory of P resulting from the PI controller experiences significant overshoot well until T reaches the desired setpoint.

2.5.1 Effect of the weighting matrix $\bar{Q}_t$ on the Lyapunov stability around the target state $\mathbf{x}_t$

Using the initial condition and operational parameters of this system presented in Table 2, the MPC and the dynamic model is constructed on the SIMULINK environment in MATLAB R2015a [40, 41]. The effects of the value of $\bar{Q}_t$ on the size of the region Ω and on the input and output sequences are considered. The target state $\mathbf{x}_t$ is chosen as $P = 500\,\text{kPa}$, and $T = 243.15\,\text{K}$. The initial condition $\mathbf{x}_0$ is chosen as $P = 300\,\text{kPa}$, and $T = 293.15\,\text{K}$. The input constraint U is defined in Eq. (2.27) such

that both m_{in} and m_{out} have nonnegative values throughout the operation. The reason that the penalty on offset of T in Q is greater than that of P comes from the analysis of Eq. (2.14). Whereas $\frac{dP}{dt}$ is less dependent on T when the tank wall is well insulated, $\frac{dT}{dt}$ is coupled with P. Thus T should be harder to control than P and therefore its offset is given a stronger penalty. A slightly greater penalty is on m_{out} because it is desirable to have a minimal value of m_{out}. The resulting weighting matrices Q and R are shown in Eq. (2.28) and the prediction horizon p is set to be 20 steps.

$$U = \left\{ \mathbf{u} \in \mathbb{R}^2 | \mathbf{u} \geq \begin{bmatrix} 0 & 0 \end{bmatrix}^T \right\} \tag{2.27}$$

$$Q = \begin{bmatrix} 0.2 & 0 \\ 0 & 1 \end{bmatrix}, \quad R = \begin{bmatrix} 0.5 & 0 \\ 0 & 0.6 \end{bmatrix} \tag{2.28}$$

To formulate the control problem shown in Eq. (2.18), the Jacobian matrix Φ is obtained by linearizing and discretizing Eq. (2.14) at $\mathbf{x}_t$ with $\Delta t = 0.5\,\text{h}$. The eigenvalues in the Eq. (2.29) indicate that the precooling process example is an integrating process at $\mathbf{x}_t$, disabling the use of the Lyapunov stability condition in Eq. (2.20).

$$\lambda(\Phi) = \begin{bmatrix} 1.0000 & 0.9930 \end{bmatrix} \tag{2.29}$$

The stability of $\mathbf{x}_t$ is confirmed with a gradient plot in Fig. 7. Since $\mathbf{x}_t$ is a critical equilibrium, $\bar{Q}_t$ is approximated suboptimally using the modified Lyapunov stability condition.

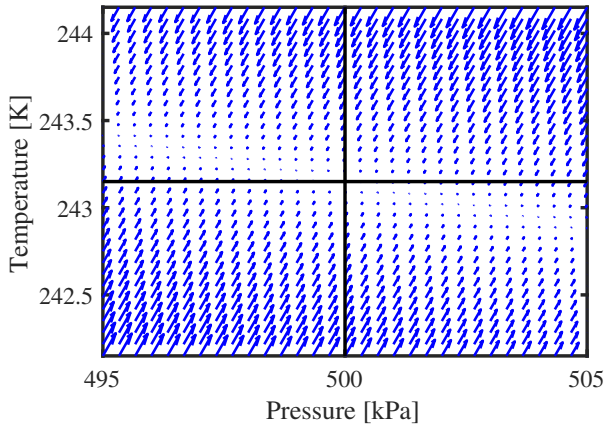

Figure 7: The gradient plot around the target state $P = 500\,\text{kPa}$, $T = 243.15\,\text{K}$

The interval $[-1 - \lambda_{\min}(\Phi), 1 - \lambda_{\max}(\Phi)]$ is divided into 400 equal segments, producing 401 different values of κ. Each κ is placed into Eq. (2.21), excluding the minimum and the maximum points, and yields $\bar{Q}_t$. Table 4 shows four cases among these κ and the corresponding eigenvalues of $\bar{Q}_t$. The region Ω around $\mathbf{x}_t$ corresponding to the cases in Table 4 is depicted in a purple color in Fig. 8. The size of Ω is the smallest in Case 1, with $\bar{Q}_t$ also being the smallest. Infeasible regions shown in a yellow color are present adjacent to $\mathbf{x}_t$, except in Case 4, in which no infeasible region is present. If the state variables exist in the yellow region, the Lyapunov stability condition becomes infeasible with $\bar{Q}_t$ and

Table 4: Change in $\lambda\left(\bar{Q}_t\right)$ with respect to the change of κ

Case	κ	$\lambda\left(\bar{Q}_t\right)$
Case 1	-1.8538	diag(0.7465, 3.8694)
Case 2	-1.9235	diag(1.4143, 7.5361)
Case 3	-1.9634	diag(3.2663, 18.0846)
Case 4	-1.9734	diag(5.0520, 28.6475)

the terminal penalty $V(\mathbf{x}_p)$ diverges. Nevertheless, we know intuitively that the state trajectories stay inside Ω if they approach $\mathbf{x}_t$ at the center in a diagonal direction starting from the upper-left corner where $\mathbf{x}_0$ is located. Therefore $V(\mathbf{x}_p)$ will remain stable in all four cases.

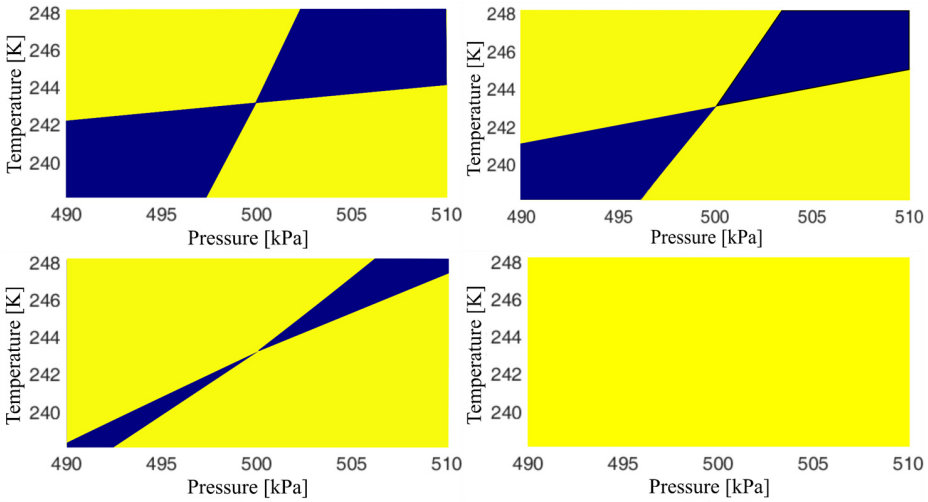

Figure 8: Change of Ω along the magnitude of $\bar{Q}_t$; (a) Case 1; (b) Case 2; (c) Case 3; (d) Case 4 (yellow zone: area where Eq. (2.20) is feasible when $Q_t = \bar{Q}_t$; purple zone: area where Eq. (2.20) is infeasible when $Q_t = \bar{Q}_t$)

2.5.2 Effect of $\bar{Q}_t$ on control input and state variable trajectories

The optimal control simulation is calculated using $\bar{Q}_t$ matrices from Table 4. The resulting input and output sequences are shown in Fig. 9. In each case, P and T of the storage tank approach the target state rapidly during the initial phase of the pre-cooling process. Although the converging speed is reduced thereafter, the calculated input sequence creates an

acceptable operation result because the pre-cooling process is completed within 15 hours, which satisfies the constraint of the operation time.

All four cases of different $\bar{Q}_t$ yield similar m_{out} sequences. The purging of the CO_2 cooling gas through the outlet does not start until $t = 2\,\text{h}$ $(k = 4)$. At this point, the increasing rate of P is sharply reduced, whereas the decreasing rate of T is maintained. The cooling power decreases as the inlet flowrate of the cooling gas starts to decline afterwards. A more significant difference is observed in the m_{in} sequences. A larger $\bar{Q}_t$ results in a larger $V(\mathbf{x}_p)$, reducing the magnitude of state and input penalty terms in Eq. (2.18). Hence, the initial value of m_{in} is larger in Case 1, resulting in a more stable input sequence than the other cases.

The maximum value of the acceptable cooling rate is approximately $-10\,\text{K/h}$. Although a constraint on the rate of change on T or an upper bound on m_{in} is not included in the control objective problem, Fig. 9 shows that the controller satisfies this condition without any constraint other than Eq. (2.27). An additional constraint may be added to the control objective problem if the maximum cooling rate exceeds $-10\,\text{K/h}$ at any time step due to the changes of the operation and control parameters or the initial condition. In this case the cooling rate can be restricted indirectly by adding an upper bound of $\mathbf{u}$ in Eq. (2.27). On the other hand if the user wants to directly restrict the value of the cooling rate by limiting the tank temperature T itself, a new type of constraint on the state variable $\mathbf{x}$, e.g. $\theta \leq \mathbf{x}_{k+1} - \mathbf{x}_k$ is required. This is a time-varying constraint involving a combination of $\mathbf{x}$ and $\mathbf{u}$ that reduces the feasible region of the control objective problem each time when the moving horizon window

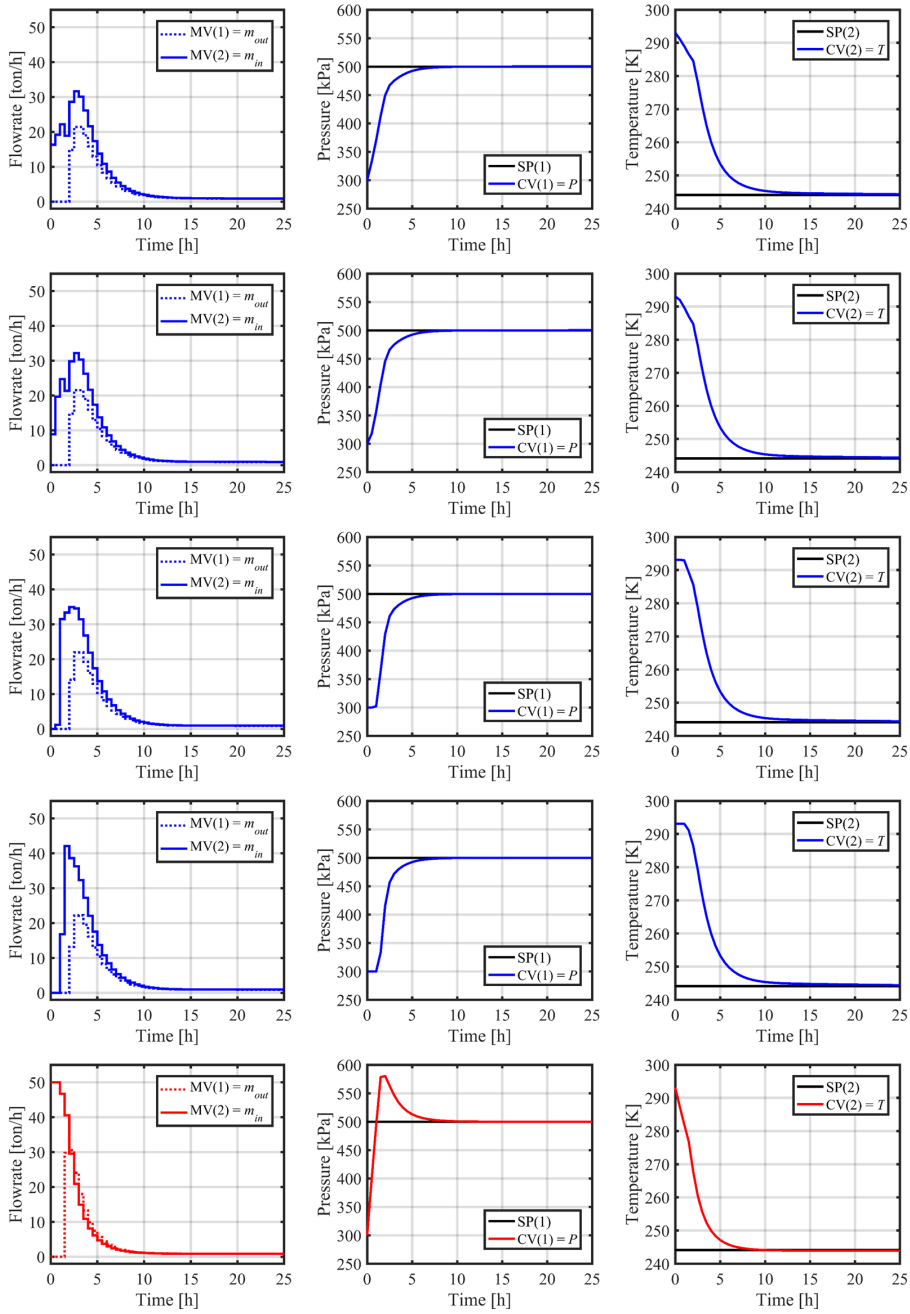

Figure 9: Dynamic sequences of outputs and control inputs; column 1: control inputs m_{in} and m_{out}; column 2: trajectory of P; column 3: trajectory of T; row 1: MPC-case 1; row 2: MPC-case 2; row 3: MPC-case 3; row 4: MPC-case 4; row 5: base case-PI control

is shifted towards the next time step. Hence, the control objective problem may become difficult for practical implementations when the state constraints are imposed.

As the magnitude of m_{in} and m_{out} with both control algorithms reach the minimum values at the end of the operation, we can conclude that the CO_2 BOG formation is restricted with a rigorous application of controllers, regardless the type of controller. Nevertheless, a noticeable difference between the results of the MPC application and the PI controller is that the control input sequence of m_{in} of the PI controller starts with a maximum value within the entire trajectory. This is due to the fact that the PI controller inherently does not take account of the interactions of P and T which are significantly related to each other when calculating the feedback control inputs. During the initial operation period when m_{in} is driven to a higher value in order to lower T, P has not yet reached the required setpoint which delays the opening of m_{out}. Thus P accumulates inside the tank system until T reaches the setpoint and there is no more need to retain m_{in} above the nominal value.

For small CO_2 storage tanks with capacities less than $1500\,\mathrm{m}^3$, the tank walls can support pressure around 14–20 bar (1400–2000 kPa) [6]. However the pressure limit tend to decrease to a lesser value as the tank storage capacities grow. For example, commercial large-capacity storage tanks for CO_2 are operated at a pressure around 5–7 bar (500–700 kPa) [42]. Although the pressure overshoot occurring during the PI control is contained within the operation pressure range for the given tank specification, this phenomenon should be avoided if possible, to secure the

overall process stability for various facility operation conditions. Also despite the initial cooling rate of the PI controller is faster than the MPC, this is unnecessary since the desirable cooling rate of the pre-cooling process has been set to -10 K/h.

Thus the MPC algorithm shows its effectiveness on the control stability compared to the PI controller by considering the multivariable interaction when calculating the future control action.

2.5.3 Discussion

In the first part of this case study, a nonlinear dynamic model of the pre-cooling process required to prevent physical damage to the CO_2 storage tank in CO_2 carriers is derived from the mass and energy balance equations of the tank unit. A closed-loop MPC algorithm is developed with this model to optimize the injection and outlet purge flowrate of the cooling gas. A terminal penalty is inserted to the objective function in order to theoretically enhance the state convergence towards the target setpoint. The second part of this study approximates a suboptimal weight matrix of the terminal penalty using the modified Lyapunov stability condition in case the target state equilibrium is not asymptotically stable. The effect of the weighting matrix of the terminal penalty on the feasible region around the target state equilibrium and the optimal input and output sequences are also discussed. Compared to the PI controller results, the MPC algorithm results show more stability led by the model-based optimization using the mathematical model. The modeling method

and the optimal control provide the pre-cooling process of a CO_2 carrier with an input sequence that reduces the vaporization waste of liquid CO_2 cargo and completes the process within the desired operation time limit.

The proposed method calculating a terminal penalty for a dynamic system handles all eigenvalues equally by indiscriminately adding an arbitrary constant on them. For a system in which an unstable eigenvalue is decoupled from other eigenvalues, an improved method providing the stability and the extra penalty on error accumulations which are out of range of the control horizon could become a subject of future studies, so that it can manipulate the problematic eigenvalue separately from the others and thus handles the issue of instability in a more sophisticated manner.

Chapter 3

Concluding remarks

3.1 Summary and contributions

This thesis presents a theoretical approach on designing the geometry of a gas cooling system unit and its application with the multivariable optimal control technique based on the dynamic mathematical models with a motivation to enhance the cooling efficiency. Two example cooling processes that are discussed in this study and come under this definition are the CO_2 storage tank pre-cooling process and the microparticle cooling process. Although both processes are included in a same process category, the individual process characteristics and their ultimate goals which need to be achieved are significantly different. Hence, such factors requiring the main consideration are discussed for the design of the cooling process units. These apply also on developing the optimal controller scheme for the gas cooling systems. Rigorous dynamic modelings are derived for each process based on the first principles which are further used in the development of appropriate model predictive control (MPC) schemes. The result produced by these optimal controllers

are later compared with base cases using the proportional-integral (PI) controllers, which illustrate that the multivariable optimal control is able to enhance the stability and the efficiency of both processes. The MPC schemes applied on each gas cooling systems are formulated with different structures and algorithms. This is because the objectives of both processes are not same as each other; one aims to reach a far-away target state with an enhanced penalty on the terminal state-setpoint error, the other targets to achieve a stable process operation by combining the optimal control algorithm with a PI control loop. Such variation on the control strategy can be achieved with a thorough study on the first-principle models, which is difficult to do so by only using the commercial simulators available in the market.

3.2 Suggested future works

Possible subjects for further studies regarding this topic are enlisted below:

1) A terminal penalty that guarantees the closed-loop stability around the target equilibrium for a discrete MPC example and has theoretically rigorous proofs could provide stronger stability than the terminal penalty obtained by the modified Lyapunov stability condition, which does not provide a generalized closed-loop stability. For continuous MPC examples the method of obtaining a stable terminal penalty has been studied deeply, but it has been significantly difficult for discrete MPC examples.

2) Scaling-up a process system having turbulent gas flow is hard if the

dimensional analysis is not possible. Hence in order to configure a system design achieving production objectives in industrial scale, alternative designing methods should be studied further. First, the user should take into account of the important physical properties and the characteristics of fluid mechanics inside the system, possibly using the artificial neural network (ANN) to configure the relationship between the system geometry and the fluid flow. Hence some meaningful geometry constraints could be deduced from this preliminary study. Utilizing this information, efficiencies of various process designs including the multiple parallel unit configuration and the single unit setting should be compared with each other to pick the best scale-up design.

3) An efficient model reduction method not only reduces significant computational power required for the original CFD simulation, but also provides useful information about the optimal sensor location of a designated process variable [43]. Model reduction algorithms such as the proper orthogonal decomposition (POD) using snapshot data or the eigensystems realization algorithm (ERA) [43, 44, 45] have been already studied in depth in attempt to replace CFD simulation in real-time optimal control problems or finding efficient sensor locations. To improve the existing researches, efficient CFD model reduction methods for complex systems having multiphase flow or chemical reactions could become a good aim.

Bibliography

[1] J.-W. Park, D.-S. Kim, M.-S. Ko, J.-H. Cho, A study on the experimental measurements and its recovery for the rate of boil-off gas from the storage tank of the CO_2 transport ship, Clean Technology 20 (1) (2014) 1–6.

[2] P. S. Fruehauf, I.-L. Chien, M. D. Lauritsen, Simplified imc-pid tuning rules, ISA Transactions 33 (1) (1994) 43–59.

[3] B. D. Tyreus, W. L. Luyben, Tuning pi controllers for integrator/dead time processes, Industrial & Engineering Chemistry Research 31 (11) (1992) 2625–2628.

[4] D. Bjerketvedt, J. R. Bakke, K. Van Wingerden, Gas explosion handbook, Journal of hazardous materials 52 (1) (1997) 1–150.

[5] A. S. Mujumdar, Handbook of industrial drying, 4th Edition, CRC Press, 2014.

[6] S. G. Lee, G. B. Choi, J. M. Lee, Optimal design and operating conditions of the CO_2 liquefaction process, considering variations in cooling water temperature, Industrial & Engineering Chemistry Research 54 (51) (2015) 12855–12866.

[7] B. Metz, O. Davidson, H. de Coninck, M. Loos, L. Meyer, Carbon dioxide capture and storage: special report of the intergovernmental panel on climate change, Cambridge University Press, 2005.

[8] B. Y. Yoo, D. K. Choi, H. J. Kim, Y. S. Moon, H. S. Na, S. G. Lee, Development of CO_2 terminal and CO_2 carrier for future commercialized CCS market, International Journal of Greenhouse Gas Control 12 (2013) 323–332.

[9] J. Y. Jung, C. Huh, S. G. Kang, Y. Seo, D. Chang, CO_2 transport strategy and its cost estimation for the offshore CCS in korea, Applied Energy 111 (2013) 1054–1060.

[10] O. Akhuemonkhan, R. R. Vara, US firm outlines its LNG terminal cool-down procedure at start-up, LNG Journal (February, 2009) 23–26.

[11] Q. S. Chen, J. Wegrzyn, V. Prasad, Analysis of temperature and pressure changes in liquefied natural gas (LNG) cryogenic tanks, Cryogenics 44 (10) (2004) 701–709.

[12] C. S. Lin, N. T. Van Dresar, M. M. Hasan, Pressure control analysis of cryogenic storage systems, Journal of Propulsion and Power 20 (3) (2004) 480–485.

[13] Praxair, Praxair cryogenic supply systems: An inside look, 39 Old Ridgebury Road, Danbury, CT 06810-5113, USA (2010).

[14] C. Harding, K. Williams, Leak detection and cool-down monitoring at LNG facilities, in: LNG 17 International Conference, Houston, 2013.

[15] G. Ransom, Pluto LNG plant start-up, in: LNG 17 International Conference, Houston, 2013.

[16] M.-J. Jung, J. H. Cho, W. Ryu, LNG terminal design feedback from operator's practical improvements, in: The 22nd World Gas Congress, Tokyo, Japan, Citeseer, 2003.

[17] S. J. Qin, T. A. Badgwell, A survey of industrial model predictive control technology, Control engineering practice 11 (7) (2003) 733–764.

[18] K. den Bakker, A step change in lng operations through advanced process control, in: 23rd World Gas Conference, Amsterdam, 2006.

[19] H. Michalska, D. Q. Mayne, Robust receding horizon control of constrained nonlinear systems, Automatic Control, IEEE Transactions on 38 (11) (1993) 1623–1633.

[20] Y. Yang, J. M. Lee, An iterative optimization approach to design of control Lyapunov function, Journal of Process Control 22 (1) (2012) 145–155.

[21] F. Dauber, R. Span, Modelling liquefied-natural-gas processes using highly accurate property models, Applied Energy 97 (2012) 822–827.

[22] N. Jang, M. W. Shin, S. H. Choi, E. S. Yoon, Dynamic simulation and optimization of the operation of boil-off gas compressors in a liquefied natural gas gasification plant, Korean Journal of Chemical Engineering 28 (5) (2011) 1166–1171.

[23] D. B. Robinson, D. Y. Peng, S. Y. K. Chung, The development of the Peng-Robinson equation and its application to phase equilibrium in a system containing methanol, Fluid Phase Equilibria 24 (1) (1985) 25–41.

[24] J. Xiao, Q. Li, D. Cossement, P. Bénard, R. Chahine, Lumped parameter simulation for charge–discharge cycle of cryo-adsorptive hydrogen storage system, International Journal of Hydrogen Energy 37 (18) (2012) 13400–13408.

[25] J. M. Smith, H. C. Van Ness, M. M. Abbott, Introduction to chemical engineering thermodynamics, 7th Edition, McGraw-Hill, 2005.

[26] R. Span, W. Wagner, A new equation of state for carbon dioxide covering the fluid region from the triple-point temperature to 1100K at pressures up to 800MPa, Journal of Physical and Chemical Reference Data 25 (6) (1996) 1509–1596.

[27] M. Morari, J. H. Lee, Model predictive control: past, present and future, Computers & Chemical Engineering 23 (4) (1999) 667–682.

[28] D. Q. Mayne, J. B. Rawlings, C. V. Rao, P. O. Scokaert, Constrained model predictive control: Stability and optimality, Automatica 36 (6) (2000) 789–814.

[29] J. B. Rawlings, Tutorial overview of model predictive control, Control Systems, IEEE 20 (3) (2000) 38–52.

[30] J. H. Lee, M. Morari, C. E. García, Model Predictive Control, Preprint, 2003.

[31] K. Zhou, J. C. Doyle, K. Glover, et al., Robust and optimal control, Vol. 40, Prentice hall New Jersey, 1996.

[32] P. Shi, E.-K. Boukas, Y. Shi, R. K. Agarwal, Optimal guaranteed cost control of uncertain discrete time-delay systems, Journal of Computational and Applied Mathematics 157 (2) (2003) 435–451.

[33] A. Visioli, Q. Zhong, Control of integral processes with dead time, Springer Science & Business Media, 2010.

[34] H. Chen, F. Allgöwer, A quasi-infinite horizon nonlinear model predictive control scheme with guaranteed stability, Automatica 34 (10) (1998) 1205–1217.

[35] G. Bitsoris, Positively invariant polyhedral sets of discrete-time linear systems, International Journal of Control 47 (6) (1988) 1713–1726.

[36] D. E. Seborg, D. A. Mellichamp, T. F. Edgar, F. J. Doyle III, Process dynamics and control, 3rd Edition, John Wiley & Sons, 2010.

[37] B. Rice, D. Cooper, Design and tuning of PID controllers for integrating (non-self regulating) processes, TECHNICAL PAPERS-ISA 422 (2002) 437–448.

[38] Y. A. Husnil, M. Lee, Control structure synthesis for operational optimization of mixed refrigerant processes for liquefied natural gas plant, AIChE Journal 60 (7) (2014) 2428–2441.

[39] S. Skogestad, P. Lundström, E. W. Jacobsen, Selecting the best distillation control configuration, AIChE Journal 36 (5) (1990) 753–764.

[40] L. Wang, Model predictive control system design and implementation using MATLAB®, Springer Science & Business Media, 2009.

[41] A. Bemporad, M. Morari, N. L. Ricker, Model predictive control toolbox, user's guide, The mathworks.

[42] I. GHG, Ship transport of co2, Cheltenham, International Energy Agency Greenhouse Gas R&D Programme.

[43] B. Apacoglu, A. Paksoy, S. Aradag, CFD analysis and reduced order modeling of uncontrolled and controlled laminar flow over a circular cylinder,

Engineering Applications of Computational Fluid Mechanics 5 (1) (2011) 67–82.

[44] S. Hovland, J. Gravdahl, K. Willcox, Explicit MPC for large-scale systems via model reduction, AIAA Journal of Guidance, Control and Dynamics 31 (4).

[45] K. Li, H. Su, J. Chu, C. Xu, A fast-POD model for simulation and control of indoor thermal environment of buildings, Building and Environment 60 (2013) 150–157.

초 록

본 논문은 기체를 제한된 공간에 주입하여 같은 공간에 유입되는 외부 열이나 미세입자 형태의 고체 물질의 열을 냉각하는 기체 냉각공정에 대해 다루고 있다. 물 또는 수증기, 에탄올 (ethanol) 을 포함하는 휘발성 냉매와 불소계 (fluorine) 물질과 달리 기체 냉각공정은 질소, 이산화탄소 및 공기와 같은 화학적으로 비활성 상태를 유지하는 유체를 냉매로 사용한다. 이러한 기체들은 냉각 대상의 특성을 보존하는 장점이 있으나 비열이 공기와 같거나 더욱 낮기 때문에 실제 운전 및 시스템 구조 설계 단계에서 다음과 같은 문제가 발생할 수 있다. 1) 냉각 효율이 다른 냉매에 비하여 떨어지기 때문에 시스템을 제외한 기타 물질을 냉각하는 경우 필요한 물질의 체류 시간을 보장할 수 있도록 냉각시스템의 크기를 증가시켜야 한다. 2) 낮은 밀도로 인해 같은 조건의 물질 또는 시스템을 냉각하기 위해 사용되는 유체 주입량이 많다. 이로 인한 시스템 내부의 압력과 냉매 공급의 증가에 따른 운전 및 관리 비용 상승을 줄일 수 있도록 냉매 주입량을 조절하는 최적 제어 기법을 공정 운전에 적용해야 한다. 이에 본 논문에서는 기체 냉각공정에 포함되는 이산화탄소 (CO_2) 저장 탱크의 예냉 (pre-cooling) 공정과 고분자 미세입자 융용 분사 (melt-spray) 공정의 후처리 단계인 냉각기 (spray cooling chamber) 공정을 예제로 하여 공정의 용도에 부합하는 체계적인 유닛 설계 방법과 공정의 동적 모델을 기반으로 하는 다변수 모델예측제어 (MPC: model predictive control) 를 적용한 안정적인 운전 전략을 제안하였다.

첫 번째 예제인 이산화탄소 저장탱크 시스템은 액화 이산화탄소 수송선의 부속시설로서, 초저온 액화 이산화탄소를 저장 주입하는 과정에서 발생할 수 있는 탱크 벽의 열적 변형을 예방하기 위해 탱크 벽면과 내부를 액화 화물과 유사한 온도까지 예냉하는 단계를 거쳐야 한다. 이 예냉공정은 액화화 이산화탄소 화물의 일부를 기화시켜 탱크에 주입함으로써 탱크 내부 온도를 낮추고 압력을 상승시키는 과정이다. 이산화탄소 저장 탱크 시스템은 예냉공정을 고려하지 않고 선박 내 선적 한계를 최대화하는 방향에서 이낭형 (bi-lobe) 구조의 $13\,000\,\mathrm{m}^3$ 규모로 사전 설계되었다. 예냉공정에 대한 모델예측제어의 적용은 탱크에 주입되어야 하는 CO_2 기체 주입량을 제한하여 CO_2 의 포집 및 액화비용의 손실을 줄이는 효과가 있다. 먼저 공정에 대한 비선형 다변수 동적 모델을 전개하여 CO_2 기체 주입유량과 배출유량을 조절하여 탱크 내 압력과 온도를 제어하는 수학적 관계를 정의하였다. 이후 유한구간 선형화 모델예측제어기 (finite-horizon linearized MPC) 를 적용하여 예냉공정을 제한 운전시간 안에 마무리하는 운전전략을 수립하였다. 적분공정 (integrating process) 인 예냉공정의 상태변수와 설정값 (setpoint) 간 오차를 줄이고 이론적으로 유한구간 최적화에 대한 안정성을 보장하기 위해 종착비용 (terminal penalty) 항을 목적함수에 추가하였다. 또한 종착비용은 변형된 리아푸노프 안정성 조건 (Lyapunov stability condition) 의 해로 차선적으로 근사되었다. 종착비용의 가중행렬 (weighting matrix) 은 복수의 해로 계산되며, 모델예측제어기의 목적함수에 관여하므로 계산되는 제어입력값과 공정출력에 영향을 주었다.

두 번째 예제인 미세입자 냉각공정 시스템은 미세 고분자입자 융용 분사 (melt-spray) 공정의 후처리 단계인 냉각기 (spray cooling

chamber) 를 포함하며, 고온에서 융용 상태로 분사되는 입자와 냉각용 공기를 함께 냉각기 내부로 분사, 혼합시켜 입자를 유리화 온도 (T_g: glassification temperature) 이하로 냉각하여 고형화하는 공정이다. 이를 수행할 수 있는 시스템을 제작하기 위해 먼저 냉각기의 구조가 노즐에서 분사되는 구형 미세입자에 충분한 입자체류시간 (PRT: particle residence time) 을 보장할 수 있도록 이론적인 설계 기준을 정립하였다. 이 과정에서 입자 크기에 따라 냉각기 높이와 나머지 설계 변수들이 입자 냉각에 미치는 영향을 분리하여 평가하였다. 일차적으로 크기가 상대적으로 큰 입자들에 한하여 노즐에서 분사된 후 충분한 입자체류시간 (PRT: particle residence time) 을 가지도록 하는 냉각기의 최소 높이를 기존 문헌에 공개된 입자 속도식과 온도식을 결합한 집중상수모델 (lumped parameter model) 을 통해 결정하였다. 냉각기 높이를 결정한 뒤, 냉각기 지름, 하단 원뿔 높이 및 냉각기 출구 지름에 따라 세분화한 냉각기 구조의 6 개 케이스를 지정하였다. 크기가 상대적으로 작은 입자의 거동은 주변 공기의 흐름과 오차가 적으므로, 케이스 별로 고온 공기의 주입유량이 변화한 이후의 구조 내부의 공기 흐름의 변화를 전산유체역학 (CFD: computational fluid dynamics) 모사를 통해 계산하는 방식으로 크기가 작은 입자의 흐름을 간접적으로 분석하여 냉각기 내부 공간에서 공기 흐름의 불안정성이 적고, 중심부와 주변부의 공기 혼합이 잘 이루어지는 냉각기 구조를 6개 케이스 중에서 선정하였다. 최종적으로 결정된 냉각기 구조 내부에서 미세입자의 냉각이 원활하게 이루어짐을 CFD 모사로 검증하였다.

다음으로 미세입자 냉각공정에 최적제어기를 적용하기 위해 입자 상태를 실시간으로 측정하기 어려우므로 냉각기 내부의 공기

상태와 외부로 배출되는 공기유량을 바탕으로 간접적으로 냉각 효율을 평가하는 방식을 사용한다. 먼저 냉각공정의 공기 유출입에 대한 다변수 동적 모델링을 전개하여 냉매로 사용되는 저온 공기와 고온 공기의 유량을 조절하여 냉각기 내부의 공기 온도와 출구를 통해 배출되는 공기 유량을 제어하는 수학적 관계를 정의하였다. 냉각기 내부의 공기 온도는 냉각효율과 입자 생산물의 품질을 결정하며, 출구 공기 유량은 냉각기 후속 공정인 입자 포집 및 크기 별 분리 공정의 운전에 영향을 미친다. 따라서 모델예측제어와 비례적분제어를 연결한 제어기를 도입하여 저온 공기의 사용량을 축소하고, 분사– 냉각– 포집 및 분리로 이어지는 연속공정의 안정적인 운전을 유도할 수 있음을 보였다.

주요어 : 예냉공정, 미세입자 냉각공정, 모델예측제어, 전산유체역학

학번 : 2010-21010